*Article*

# The Impact of Eclipsing GNSS Satellites on the Precise Point Positioning

**Xinyun Cao [1,2]** (iD)**, Shoujian Zhang [1,\*], Kaifa Kuang [1,2], Tianjun Liu [3] and Kang Gao [1,2]**

[1]  School of Geodesy and Geomatics, Wuhan University, 129 Luoyu Road, Wuhan 430079, China;
    xycao@whu.edu.cn (X.C.); kfkuang@whu.edu.cn (K.K.); whurinex@163.com (K.G.)
[2]  Key Laboratory of Geophysical geodesy, National Administration of Surveying,
    Mapping and Geoinformation, Wuhan University, 129 Luoyu Road, Wuhan 430079, China
[3]  School of Environment and Spatial Informatics, China University of Mining and Technology,
    1 Daxue Road, Xuzhou 221116, China; tjliu_cumt@126.com
\*   Correspondence: shjzhang@sgg.whu.edu.cn; Tel.: +86-13437272488

**Abstract:** When satellites enter into the noon maneuver or the shadow crossing regimes, the actual attitudes will depart from their nominal values. If improper attitude models are used, the induced-errors due to the wind-up effect and satellite antenna PCO (Phase Center Offset) will deteriorate the positioning accuracy. Because different generations of satellites adopt different attitude control models, the influences on the positioning performances deserve further study. Consequently, the impact of three eclipsing strategies on the single-system and multi-GNSS (Global Navigation Satellite System) Precise Point Positioning (PPP) are analyzed. According to the results of the eclipsing monitor, 65 globally distributed MGEX (Multi-GNSS EXperiment) stations for 31-day period in July 2017 are selected to perform G/R/E/C/GR/GREC PPP in both static and kinematic modes. The results show that the influences of non-nominal attitudes are related to the magnitude of the PCO values, maximum yaw angle differences, the duration of maneuver, the value of the sun angle and the satellite geometric strength. For single-system, using modeled attitudes rather than the nominal ones will greatly improve the positioning accuracy of GLONASS-only and BDS-only PPP while slightly contributions to the GPS-only and GALILEO-only PPP. Deleting the eclipsing satellites may sometimes induce a longer convergence time and a worse solution due to the poor satellite geometry, especially for GLONASS kinematic PPP when stations are located in the low latitude and BDS kinematic PPP. When multi-GNSS data are available, especially four navigation systems, the accuracy improvements of using the modeled attitudes or deleting eclipsing satellites are non-significant.

**Keywords:** attitude control model; yaw steering mode; orbit normal mode; multi-GNSS; precise point positioning

## 1. Introduction

The satellite attitudes usually satisfy two basic requirements: the transmitting navigation antenna is pointing towards to the geocenter and the solar panel axis is perpendicular to the incident direction of the sun. These two requirements can be realized by the satellite Attitude Control Subsystem (ACS) using solar sensors mounted on the solar panels. The nominal yaw attitude is defined by the satellite body-fixed axes: the *Z*-axis is pointing towards the geocenter, the *Y*-axis is parallel to the rotation axis of the solar panels, and then the *X*-axis completes the right-handed coordinate system. Most of the time, the satellite can remain the nominal attitude. However, two singularities when satellite–earth–sun are collinear have broken down the nominal attitude, causing two 180° discontinuities. At this time, the satellite will experience noon maneuver, shadow crossing or post-shadow recovery until the actual

yaw angle is equal to its nominal value [1]. Since the body-fixed *Z*-axis is always pointing to the earth, the determination of the attitude is mainly to determine the orientation of body-fixed *X*-axis.

The attitude of GNSS satellites are the critical information for GNSS Precise Orbit Determination (POD) and PPP. The influences of the attitude mainly include three aspects: the solar radiation pressure model, the phase wind-up model and the corrections of the antenna PCO. Since the POD is beyond the scope of this contribution, only the latter two aspects are considered. When the orbit products are referred to the Center of Mass (CoM), the corrections of the antenna PCO should be required [2]. In general, the post-processing orbit products are referred to the CoM. For the real-time products, as in case of CNES real-time multi-GNSS corrections (https://igsac-cnes.cls.fr/), the values are referred to the satellite antenna phase center and only the phase wind-up corrections are needed. The wind-up corrections because of the attitude error can reach up to 10 cm. While the magnitude of the corrections of PCO because of the attitude error is closely related to the magnitude of the antenna eccentricity in X and Y direction. This error does not exist for GPS IIR-A/IIR-B/IIR-M and GLONASS-K1 satellites since their horizontal antenna eccentricity is near-zero. However, this error should be carefully considered for GPS IIF, GLONASS-M and all BDS satellites [3].

In recent years, GNSS has developed towards a new stage with more systems and frequencies [4]. Different types of satellites usually adopt different attitude control models [3]. Therefore, it is necessary to establish the proper attitude model for different satellite types. For GPS II/IIA satellites, a rigorous deterministic model, called GYM95 (GPS Yaw attitude Model-95), for noon maneuver and shadow crossing was developed [1]. During the period of the post shadow recovery, deleting 30 min of data was recommended because of the unpredictable yaw attitude. A simplified yaw attitude model, consistent with GYM95, was implemented for GPS II/IIA and IIR satellites [5]. The attitude of GPS IIF satellites was analyzed by Reverse Kinematic Precise Point Positioning (RKPPP) and the anomalous noon turn directions for small negative sun angles ($\geq -0.9°$) had been found [6,7]. The modeled and estimated yaw angles of eight GPS IIF satellites with small sun angles were compared by RKPPP [8]. It had been found that all the GPS IIF satellites with sun angles smaller than $-0.7°$ had the correct noon turn directions with only two exceptions (both for SVN62). For GLONASS-M satellites, the attitude model for noon maneuver and shadow crossing was different from GPS satellites [9]. The Galileo IOV (In-Orbit Validation) satellites metadata and the official attitude law of GALILEO FOC (Full Operational Capability) satellites were released and updated on 6 October 2017 [10]. Different from GPS/GLONASS/GALILEO satellites, two types of attitude modes were adopted for BDS-2 satellites: yaw-steering mode and orbit normal mode. Al GEO (Geostationary Orbits) satellites will always use the orbit normal mode while the IGSO (Inclined Geosynchronous Orbit) and MEO (Medium Earth Orbit) satellites will experience the switch of attitude mode when the sun angle is below the threshold of about 4° [11,12]. Compared with BDS-2 satellites, the BDS-3 experimental satellites (5 IGSO/MEO satellites) did not use orbit normal mode anymore and adopted another threshold of about 3° for noon and midnight maneuver [13]. Since few stations can track the signals of BDS-3 satellites, only BDS-2 satellites are considered in the following experiment and analysis.

However, the previous studies mainly focus on the POD and the establishment of the attitude control model. At the same time, PPP has been widely used for scientific research and civilian applications [14–17]. To obtain high precise and reliable positioning performance, the impact of eclipsing satellites on PPP should also be understood. The positioning errors resulting from different GPS satellite types during eclipsing periods have been analyzed [18]. The results showed that the positioning accuracy could be improved by 20–30% with the modeled attitude, especially when more GPS IIA satellites were in eclipse. However, the GPS IIA satellites had been removed from GPS constellation in early 2016 [19]. Therefore, the new analysis for current GPS constellation should be also necessary. Without doubt, the introduction of multi-GNSS will significantly improve the convergence time and the positioning reliability [20–22]. Therefore, the impact of GNSS eclipsing satellites on the GNSS PPP needs further analysis, which is also the purpose of this paper.

This paper is divided into four sections. Following the Introduction, the materials and methods are given in Section 2, including the attitude model for GNSS satellites and the GNSS PPP model. Subsequently, Section 3 compares the positioning performance of three eclipsing strategies for the single-system and multi-GNSS PPP. Finally, the main points and the conclusions are summarized.

## 2. Materials and Methods

### 2.1. The Attitude Model for GNSS Satellites

The nominal yaw angle $\varphi_n$ can be computed by the sun angle $\beta$ (the elevation angle of the sun above the orbital plane [23], $-90°–90°$) and the orbit angle $\mu$ (the geocentric angle between the sun and orbit midnight, growing with the satellite motion, $0–360°$):

$$\varphi_n = \text{atan2}(-\tan\beta, \sin\mu), \tag{1}$$

where the function atan2(y, x) in C/C++ returns the principal value of the arc tangent of y/x, expressed in radians (in the interval $[-\pi, \pi]$). According to the current IGS convention, the unit vector of sun and the *X*-axis direction of the yaw-steering frame are always pointing towards the same hemisphere, including GPS IIR and GALILEO satellites [3]. Therefore, Equation (1) is used for all GNSS satellites to calculate the nominal yaw angles and the sign of $\phi_n$ is opposite to that of $\beta$.

Ignoring the small time variation of the sun angle $\beta$, the yaw rate $\dot{\varphi}_n$ can be derived as follows:

$$\dot{\varphi}_n = \frac{\dot{\mu}\tan\beta\cos\mu}{\sin^2\mu + \tan^2\beta}, \tag{2}$$

where $\dot{\mu}$ denotes the orbital angular velocity. According to the orbital period, the average orbital angular velocities for GNSS are summarized in Table 1. Substituting $\mu = 0$ and the maximum hardware yaw rate $R$ into Equation (2), the approximate maximum sun angle limit $\beta_0$ can be expressed as follows:

$$\beta_0 = \text{atan}(\dot{\mu}/R), \tag{3}$$

where the function atan(x) in C/C++ returns the arc tangent of x, expressed in radians (in the interval $[-\pi/2, \pi/2]$). For GPS II/IIA satellites, the averaged JPL reprocessing yaw-rate solutions during 1996–2008 [24] are provided, with the average value of $0.1176°/s$ ($0.0815°/s–0.1401°/s$). The average hardware yaw rate for GPS IIR, GPS IIF and GLONASS-M satellites are $0.20°/s$, $0.11°/s$ and $0.25°/s$, respectively. Different from GPS and GLONASS satellites, the GALILEO (IOV and FOC) and BDS (IGSO and MEO) satellites adopt the fixed threshold values. Then, the sun angle limits of noon maneuver are showed in the second column of Table 2. Only when the satellite moves to near the noon and $|\beta| \leq \beta_0$, it will experience noon maneuver or switch to orbit normal mode (BDS MEO and IGSO satellites).

Different from the noon maneuver, as soon as the satellite enters into the shadow regime, the solar sensors of some satellites are unable to perceive the position of the sun. According to the mean radius of earth and the altitude of the satellite orbit, the average sun angle limits for shadow crossing regime are shown in the third column of Table 2. It is noteworthy that only the midnight maneuver is considered during the shadow crossing regime for GPS IIR and GALILEO (IOV and FOC) satellites. At this time, a smaller value of $\beta_0$ causes a shorter period of shadow crossing. Except for GPS II/IIA satellites, there is no post-shadow recovery for other satellite types, including GPS IIF satellites. It is recommended to delete the 30 min of data for GPS II/IIA satellites after the exit of shadow crossing.

Different from GPS/GLONASS/GALILEO satellites, BDS satellites adopt the yaw steering mode and orbit normal mode. It is important to know the attitude switching time because of the big differences of yaw angle between these two attitude modes (the yaw angle is always 0 for orbit

normal mode). Considering that the yaw angle cannot complete an abrupt change in a short time, the preliminary attitude switch model, established by Dai et al. [12], is adopted in this contribution:

- The condition for YS- > ON: (1) $|\beta| \leq 4°$ and $|\varphi_n| \leq 5°$; or (2) $|\beta| \leq 4°$ and $5° < |\varphi_n| < 20°$ when $\varphi_n \dot{\varphi}_n > 0$.
- The condition for ON- > YS: (1) $|\beta| > 4°$ and $|\varphi_n| \leq 5°$; or (2) $|\beta| > 4°$ and $5° < |\varphi_n| < 20°$ when $\varphi_n \dot{\varphi}_n > 0$.

When the satellite enters into the noon maneuver or shadow crossing regime, the actual yaw angle can be modeled according to different attitude models [5,6,9,10,12]. In this contribution, the process of the acceleration of hardware yaw angle during the noon maneuver and the shadow crossing is ignored. The details and the results of the modeled yaw angles in this contribution are shown in Section 3.2.

When the satellites enter into the eclipsing regimes, if the nominal yaw angle is used instead of the actual one, the induced-errors of the wind-up effect and antenna PCO will deteriorate the positioning accuracy, especially when $\beta$ is small. These errors, especially the antenna PCO, can also be reflected in the phase observation residuals.

**Table 1.** GNSS orbits and attitude mode (*i*: orbital inclination, *T*: orbital period, $\dot{\mu}$: average orbital angular velocity, YS: yaw-steering, ON: orbit normal).

| Constellation | *i* | *T* | $\dot{\mu}$ | Attitude |
|---|---|---|---|---|
| GPS | 55° | 11 h 58 min | 0.00836°/s | YS |
| GLO | 65° | 11 h 16 min | 0.00888°/s | YS |
| GAL | 56° | 14 h 05 min | 0.00710°/s | YS |
| BDS-GEO | ≈0° | 23 h 56 min | 0.00418°/s | ON |
| BDS-IGSO | 55° | 23 h 56 min | 0.00418°/s | YS/ON |
| BDS-MEO | 55° | 12 h 53 min | 0.00776°/s | YS/ON |

**Table 2.** The average threshold value for different periods of GNSS attitude mode.

| Constellation | Noon Maneuver | Shadow Crossing | Post-Shadow Maneuver |
|---|---|---|---|
| GPS-II/IIA | Yes [1], $|\beta| \leq 2.39°$–5.69° [2] | Yes, $|\beta| \leq 13.5°$ | Yes |
| GPS-IIR | Yes, $|\beta| \leq 2.39°$ | Yes, $|\beta| \leq 2.39°$ [3] | No |
| GPS-IIF | Yes, $|\beta| \leq 4.34°$ | Yes, $|\beta| \leq 13.5°$ | No |
| GLO-M | Yes, $|\beta| \leq 2.03$ | Yes, $|\beta| \leq 14.2°$ | No |
| GAL-IOV | Yes, $|\beta| \leq 2.0°$ | Yes, $|\beta| \leq 2.0°$ | No |
| GAL-FOC | Yes, $|\beta| \leq 4.1°$ | Yes, $|\beta| \leq 4.1°$ | No |
| BDS-GEO | ON [4] | ON | ON |
| BDS-IGSO/MEO | ON, $|\beta| \leq 4.0°$ | ON, $|\beta| \leq 4.0°$ | ON, $|\beta| \leq 4.0°$ |

[1] Yes means that this type of satellites will experience the specified maneuver while No is the opposite. [2] The angle sun limits for GPS II/IIA satellites are computed according to the averaged JPL reprocessing yaw-rate solutions. [3] The shadow crossing for GPS IIR satellites is equivalent to the midnight maneuver. [4] The BDS GEO satellites always use the orbit normal mode.

### 2.2. The Multi-GNSS Precise Point Positioning and Its Strategy

The traditional PPP model adopts Ionosphere-Free (IF) combinations to eliminate the first-order ionospheric delays, which amounts to ignoring the spatial and temporal characteristics of the ionospheric delays. The corresponding observations of dual-frequency IF combinations are presented as follows:

$$P_{r,if}^{sys,s} = \boldsymbol{u}_r^{sys,s} \Delta \boldsymbol{x}_r + m_r^{sys,s} Z_r + dt_r^{sys} - dt^{sys,s} + O_{r,if}^{sys,s} + b_{r,if}^{sys,s} - b_{,if}^{sys,s} + \varepsilon_{P,r,if}^{sys,s}, \tag{4}$$

$$L_{r,if}^{sys,s} = \boldsymbol{u}_r^{sys,s} \Delta \boldsymbol{x}_r + m_r^{sys,s} Z_r + dt_r^{sys} - dt^{sys,s} + O_{r,if}^{sys,s} + W_{r,if}^{sys,s} + \lambda_{,if}^{sys,s} N_{r,if}^{sys,s} + B_{r,if}^{sys,s} - B_{,if}^{sys,s} + \varepsilon_{L,r,if}^{sys,s}, \tag{5}$$

where $P_{r,if}^{sys,s}$ (m) and $L_{r,if}^{sys,s}$ (m) are the observed-minus-computed pseudorange and phase observables after correcting necessary errors for satellite s and receiver r, respectively; the superscript "sys" denotes satellite system according to RINEX version 3.03 [25] (G = GPS, R = GLONASS, E = GALILEO, C = BDS); $u_r^{sys,s}$ is the linearized vector from satellite s to receiver r and $\Delta x_r$ (m) is the coordinate increment vector with respect to the priori value; $Z_r$ (m) is the zenith tropospheric wet delay for receiver r and $m_r^{sys,s}$ is its corresponding mapping function; $dt_r^{sys}$ (m) and $dt^{sys,s}$ (m) are the frequency-independent clock offsets for receiver $r$ and satellite $s$, respectively; $\lambda_{,if}^{sys,s}$ denotes the wavelength; $N_{r,if}^{sys,s}$ (cycle) is the float ambiguity due to the assimilation of the hardware delays; $O_{r,if}^{sys,s}$ (m) is the satellite PCO correction which influences both the pseudorange and phase observables, while the wind-up correct $W_{r,if}^{sys,s}$ (m) only influences the phase observables; $b_{r,f}^{sys,s}$ (m) and $b_{,f}^{sys,s}$ (m) are the pseudorange hardware delays of the IF combination for receiver $r$ and satellite $s$, respectively; $B_{r,f}^{sys,s}$ (m) and $B_{,f}^{sys,s}$ (m) are the phase hardware delays of the IF combination for receiver $r$ and satellite $s$, respectively; and $\varepsilon_{P,r,if}^{sys,s}$ (m) and $\varepsilon_{L,r,if}^{sys,s}$ (m) are the unmodeled errors in the pseudorange and phase observables, respectively. Without considering the pseudorange Inter-Frequency Biases (IFBs) of GLONASS, the pseudorange hardware delays of receiver can be treated as satellite-independent [26]. During the subsequent derivation, $b_{r,f}^{sys}$ is used instead of $b_{r,f}^{sys,s}$.

To solve the rank deficiency caused by the correlations between the clock parameters and hardware delays, in general, the new reparameterized clock is defined:

$$d\bar{t}^{sys,s} = dt^{sys,s} + b_{,if}^{sys,s}, \tag{6}$$

$$d\bar{t}_r^{sys} = dt_r^{sys} + b_{r,if}^{sys}, \tag{7}$$

at this time, the pseudorange hardware delays absorbed into the clock parameters are introduced to the phase observations. Therefore, the new float ambiguity parameters $A_{r,f}^{sys,s}$ can be expressed as the linear combination of the ambiguities and the hardware delays:

$$A_{r,f}^{sys,s} = \lambda_{,if}^{sys,s} N_{r,if}^{sys,s} + B_{r,if}^{sys,s} - B_{,if}^{sys,s} - (b_{r,if}^{sys} - b_{,if}^{sys,s}), \tag{8}$$

Instead of estimating one receiver clock for one satellite system, an alternative method is to introduce Inter-System Biases (ISBs) to compensate for the time differences among GNSS and GPS is selected as the reference in the GNSS PPP processing.

$$ISB_r^{G*} = d\bar{t}_r^* - d\bar{t}_r^G = \left(dt_r^* - dt_r^G\right) + \left(b_{r,if}^* - b_{r,if}^G\right), \tag{9}$$

where the superscript "*" denotes the abbreviation for satellite systems. The estimable ISBs parameters not only contain the true system time differences, but also the differences of hardware delays of the IF combinations. Eventually, the full rank GNSS PPP model using IF combinations are obtained:

$$P_{r,if}^{sys,s} = u_r^{sys,s} \Delta x_r + m_r^{sys,s} Z_r + d\bar{t}_r^{sys} - d\bar{t}^{sys,s} + O_{r,if}^{G,s} + ISB_r^{G*} + \varepsilon_{P,r,if}^{G,s}, \tag{10}$$

$$L_{r,if}^{sys,s} = u_r^{sys,s} \Delta x_r + m_r^{sys,s} Z_r + d\bar{t}_r^{sys} - d\bar{t}^{sys,s} + O_{r,if}^{sys,s} + W_{r,if}^{sys,s} + A_{r,if}^{sys,s} + ISB_r^{G*} + \varepsilon_{L,r,if}^{sys,s}, \tag{11}$$

When multi-GNSS data are available, the prior variance of observations are given as follows [27]:

$$\sigma^2 = \sigma_0^2 \left(1 + 1/\sin^2 e\right), \tag{12}$$

where $e$ is the satellite elevation. The value of $\sigma_0$ for GPS/GALILEO can be set as 0.003 m and 0.3 m for the raw pseudorange and phase observables, respectively. Due to the neglect of the pseudorange IFBs, the value of $\sigma_0$ for GLONASS pseudorange observables is enlarged by several times [26], such as 0.9 m. The phase IFBs of GLONASS can be absorbed by the GLONASS float ambiguities; therefore,

the value of $\sigma_0$ for GLONASS phase observables can be set as the same as that of GPS [26]. For BDS GEO satellites, because of the low accuracy of the orbit and clock products, the value of $\sigma_0$ for GEO can be set as 1.2 m and 0.009 m for the raw pseudorange and phase observables [27,28]. Due to the satellite-induced code variations for BDS IGSO and MEO satellites, the value of $\sigma_0$ for IGSO/MEO can be set as 0.4 m after correcting the satellite-induced code errors using the linear interpolation model [29]. The phase observables of IGSO and MEO satellites are not influenced by these errors and the value of $\sigma_0$ for IGSO/MEO phase observables can also be set as the same as that of GPS [27].

During the data pre-processing, data integrity, pseudorange gross errors [30] and cycle-slips [31] are checked and detected. When cycle slip occurs, new ambiguity parameters are introduced into the filter state rather than being repaired. However, the pre-processing is difficult to detect the small cycle-slips and code gross errors. To reduce the influence of the undetected cycle slips and gross errors, the robust Kalman filter using IGG (Institute of Geodesy and Geophysics) III function [32] based on the observation residuals is used to adjust the variance of the observations:

$$\bar{\sigma}^2 = \sigma^2/\gamma, \tag{13}$$

$$\gamma = \begin{cases} 1 & |\tilde{v}| \leq k_0 \\ \frac{k_0}{|\tilde{v}|}\left(\frac{k_1 - |\tilde{v}|}{k_1 - k_0}\right)^2 & k_0 < |\tilde{v}| \leq k_1 \\ 0 & |\tilde{v}| > k_1 \end{cases}, \tag{14}$$

where $\bar{\sigma}^2$ is the equivalent variance and $\gamma$ is the variance inflation factor; $|\tilde{v}|$ is the standardized residual; and $k_0$ and $k_1$ are the threshold, which are usually chosen as 1.5 and 3.0, respectively. For each iteration, only the satellite with the maximum standardized residual is selected to adjust its variance. When the standardized residual of phase observable is bigger than $k_1$, the ambiguity of this satellite is reset as a new parameter, rather than setting its variance as a large value.

The strategy of GNSS PPP is summarized in Table 3. Multi-GNSS precise orbit and clock products from GFZ/Wuhan University are used. Due to the small higher-order ionospheric delays, the higher-order corrections are ignored in all PPP schemes. Currently, the phase center corrections of receiver for GALILEO and BDS are still unavailable. Therefore, the corrections of receiver PCO and PCV (Phase Center Variations) for GALILEO and BDS are assumed the same as that of GPS. After fixing the orbit, clock and DCBs for all visible satellites, the estimable parameters for GNSS PPP are $\left(\Delta x_r, Z_r, d\bar{t}_r^G, A_{r,if}^{sys,s}, ISB_r^{G*}\right)$. The process noise of the Kalman filter state is also shown in Table 3.

**Table 3.** The GNSS PPP model and its strategy.

| Item | Models |
|---|---|
| Observations | G: L1 and L2; R: L1 and L2; E: L1 and L5; C: L2 and L7 |
| Models | Traditional IF combination |
| Estimator | Robust Kalman filter |
| Sampling rate | 30 s |
| Cut-off angle | 7° |
| Observation weight | Elevation-dependent weight |
| Satellite orbit and clock | The products of GBM are used for GPS/GLONASS/GALILEO, while the products of WUM are used for BDS |
| Eclipse strategy | S1:deleted eclipsing satellites; S2: adopted nominal attitude; S3: adopted modeled attitude |
| A Priori troposphere | GPT2 model and VMF mapping function were applied [33]; Not considering the tropospheric gradient |
| Ionosphere | The first order of the ionospheric delays is eliminated by IF combination; Not considering the higher-order delays [34] |

**Table 3.** *Cont.*

| Item | Models |
|---|---|
| Satellite antenna phase center offset | PCO and PCV values for GPS /GLONASS/GALILEO from igs.atx were used; Corrections for BDS adopted the values provided by WHU [35]; |
| Receiver antenna phase center offset | PCO and PCV values for GPS and GLONASS from igs.atx were used; Corrections for GALILEO/BDS were assumed the same as that of GPS; |
| Tidal effects | Solid tides, ocean tide loading and polar tides (IERS 2010 [36]) |
| Wind-up effect | Corrected [37] |
| Satellite DCB | Corrected by MGEX DCB products (DLR) [38] |
| Station coordinate | Estimated as constant/white noise ($10^4$ m$^2$) in static/kinematic modes |
| Zenith wet tropospheric delay | Estimated as random-walk model ($5 \times 10^{-8}$ m$^2$/s) |
| Receiver clock | Estimated as white noise ($10^4$ m$^2$) |
| Receiver ISBs | Estimated as 1-day constant |
| Phase ambiguity | Estimated as float constant for each arc; when cycle-slip happened, estimated as white noise model ($10^4$ m$^2$) |

## 3. Results and Discussion

### 3.1. Current GNSS Constellations and the Results of Eclipsing Monitor

The sun angles and the nominal yaw angles of all GNSS satellites are calculated every 30 s using precise orbit and clock products. After monitoring the sun angles and the orbital angles for all GNSS satellites, it has been found that many satellites are in eclipsing seasons in July 2017 (31 days in total, from DOY 182 to DOY 212 of 2017), as shown in Figure 1. In this month, about 85 GPS/GLONASS/GALILEO/BDS satellites are available, while 18 of them are in eclipse. Therefore, the data of this whole month are selected.

During the whole month, 31 GPS satellites are operational (except G04), including eight IIR-A satellites, four IIR-B satellites, seven IIR-M satellites and 12 IIF satellites. There are seven GPS eclipsing satellites, including two IIR satellites (in cyan dots) and five IIF satellites (in red dots). Among them, G01, G02, G06 and G21 have the complete eclipsing period in this month. Due to the smaller threshold value of the sun angle, it is obvious that the number of days influenced by the eclipsing satellites for GPS IIR satellites is significantly shorter than that of the GPS IIF satellites.

For GLONASS, the constellation is mainly composed of the GLONASS-M satellites, but also includes two GLONASS-K1 satellites [39] (R09/R26). Since the R26 satellite is in the flight test phase, no precise orbit and clock products are available. Therefore, this satellite will be automatically deleted in the PPP processing. Compared with GPS satellites, the sun angle limit of GLONASS for shadow crossing regime is relatively bigger, and R10, R11, R13, R15 and R16 satellites are always in eclipse in the whole month (in blue dots).

The GALILEO system consists of two generations of satellites, namely the IOV and FOC satellites. On 15 December 2016, GALILEO started offering Initial Operational Capability (IOC) with four IOV satellites and 14 FOC satellites (https://www.gsc-europa.eu/). Among them, the E20 (IOV) experienced a permanent failure of the E5 and E6 signal transmission and two FOC satellites (E14 and E18) were in the wrong orbits. On July 2017, four FOC satellites are in eclipse (E01/E02/E24/E30, in pink dots).

The development of BDS is divided into two stages: the regional system, which was realized at the end of December 2012, and the global system. As of July 2017, five GEO, six IGSO and three MEO satellites are providing valid navigation messages. Even though five BDS-3 satellites are successfully launched into the correct orbit plane, they are still in the phase of the flight test. Therefore, all the results of BDS satellites in this paper are always referred to that of the BDS-2 satellites. The attitude of two IGSO satellites (C07/C10, in green dots) will switch to orbit normal mode.
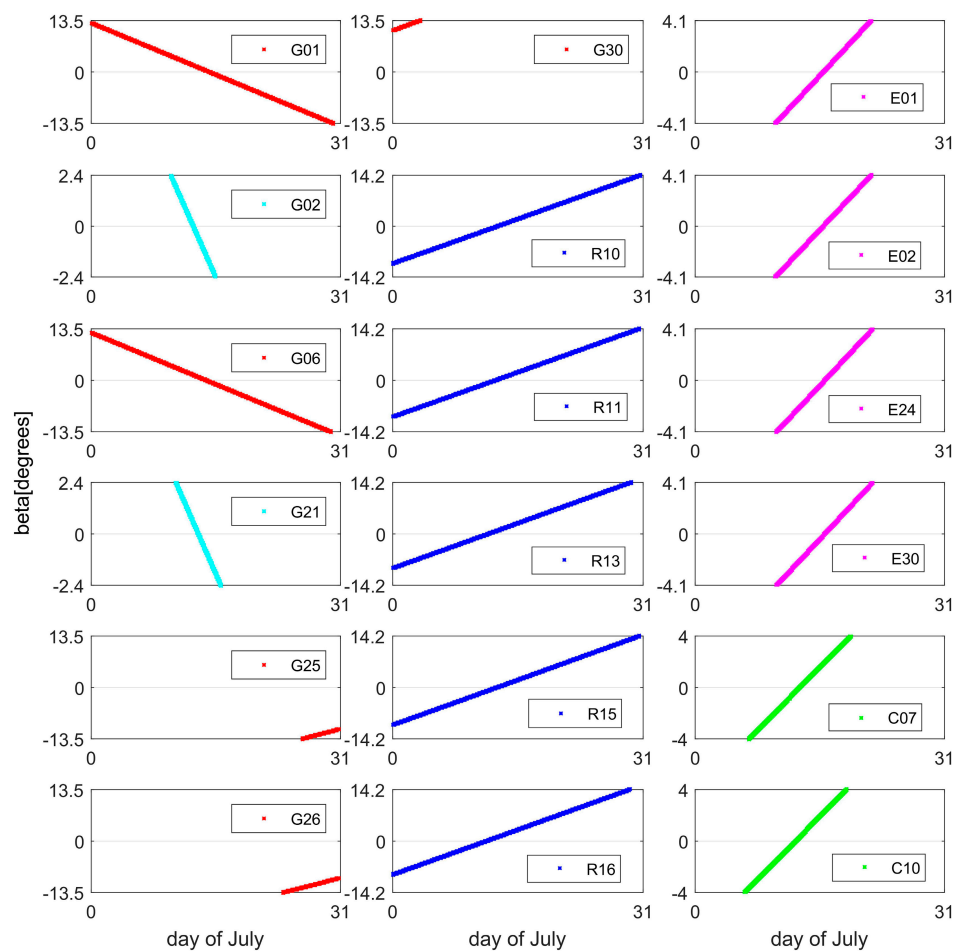
**Figure 1.** The monitoring results of the eclipsing satellites in July 2017.

Since the satellite PCO errors induced by the non-nominal yaw attitude are related to the magnitude of the PCO, the average values of GNSS satellite PCO from igs.atx are listed in Table 4. The mean values are calculated by all the current operational satellites (July 2017) with the same generation. The satellite PCO errors induced by the non-nominal yaw attitude of GPS IIF, GLONASS-M and BDS satellites are the largest, followed by the GALILEO satellites. For the GLONASS-K1 and GPS IIR satellites, the satellite PCO errors caused by the non-nominal attitude can be neglected.

**Table 4.** The average antenna phase offset for GNSS satellites (unit: mm).

| Constellation | Type | x | y | z |
|---|---|---|---|---|
| GPS | IIR-A | +2.5 | −0.8 | +1270.0 |
| | IIR-B | +5.8 | +1.8 | +788.4 |
| | IIR-M | +3.4 | +0.5 | +782.3 |
| | IIF | +394.0 | 0.0 | +1505.5 |
| GLO | M | −545.0 | 0.0 | +2396.2 |
| | K1 (R09/R26) | 0.0 | 0.0 | +2083.0/+2014.7 |
| GAL | IOV | −170.0 | +30.0 | +950.0 |
| | FOC | +120.0/+160.0 [1] | −10.0/−10.0 | +1100.0/+1050.0 |
| BDS | GEO | +600.0 | 0.0 | +1100.0 |
| | IGSO | +588.7 | 0.0 | +2902.4 |
| | MEO | +575.0 | 0.0 | +2128.0 |

[1] The PCO for E14/E18: (+160.0, −10.0, +1050.0).

## 3.2. The Yaw Angle Differences and the Duration of Eclipse

### 3.2.1. GPS IIR and IIF Satellites

When the satellites are in eclipse, the actual yaw angle or the modeled yaw angle will depart from the nominal one. First, the differences between the modeled and the nominal yaw angle of the GPS IIR satellites are analyzed. Only the differences during noon maneuver are shown in Figure 2 because of the similar results of the shadow crossing (midnight maneuver). With the decrease of the sun angle, as shown in Figure 2a–c, the differences become larger and the duration of the noon maneuver becomes shorter. The maximum differences and the duration are also listed in Table 5. When the mean sun angle is −0.08° in Figure 2c, the difference can be up to around 131.87° and the duration can be up to around 14 min.
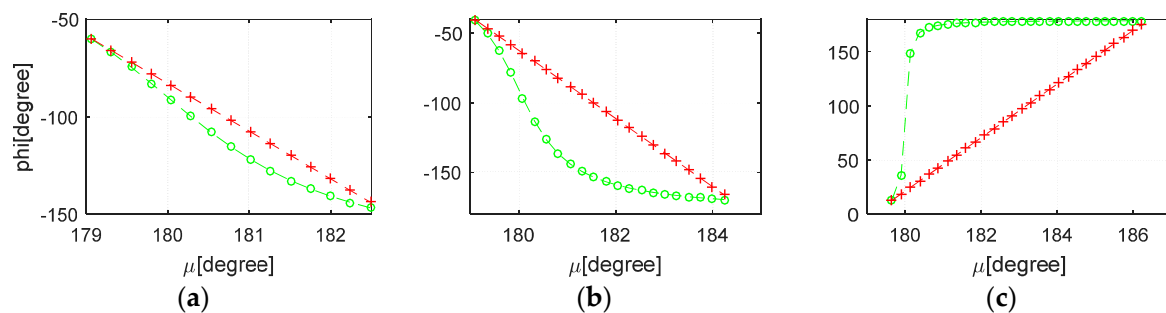


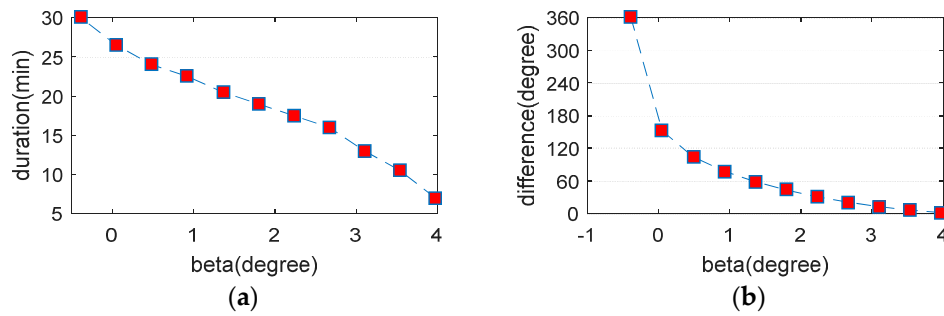**Figure 2.** The yaw angle of G21 (IIR) during noon maneuver for different sun angles: (**a**) beta = 1.63°; (**b**) beta = 0.77°; and (**c**) beta = −0.08°. The nominal yaw angle is shown in green, while the modeled one is in red.

**Table 5.** The maximum differences and duration for different sun angles (G21).

| Beta | Max Differences | Duration |
|------|-----------------|----------|
| 1.63° | 13.51° | 7.5 min |
| 0.77° | 55.75° | 11 min |
| −0.08° | 131.87° | 14 min |

For the GPS IIF satellites, as shown in Table 2, the threshold value of the sun angle for the noon maneuver is nearly twice than that of the IIR satellites. Therefore, the duration of the noon maneuver for GPS IIF satellites are longer. The duration and the difference of G06 for different sun angles, from −0.38° to 3.97°, are shown in Figure 3. Similar to IIR satellites, the differences become larger and the duration of the noon maneuver becomes shorter when the sun angle goes smaller. It is important to note that there is an anomalous IIF noon maneuver for small negative sun angle (−0.38° for G06 on 15 July 2017) because of the negative yaw bias. At this time, the opposite noon turn direction makes the angle differences up to 360° and the duration is up to approximately 30 min.

When the IIF satellites enter into the shadow crossing regime, the yaw rate (about 0.06°/s) will be computed to ensure that at the shadow exit the nominal yaw angle is reached. Due to the large sun angle limit (13.5°) for the shadow crossing, the duration is relatively long. According to the average orbital angular velocities of GPS (0.00836°/s), the maximum duration is about 54 min. However, the yaw angle differences are usually smaller than 20° when the sun angle is bigger than 5°. For example, the maximum angle differences in Figure 4a–c are 21.58°, 43.51° and 74.51°, respectively.

**Figure 3.** The duration and the yaw angle difference of G06 (IIF) during noon maneuver for different sun angles ($-0.38°$–$3.97°$): (**a**) the duration; and (**b**) the difference between the nominal yaw angle and the modeled yaw angle.
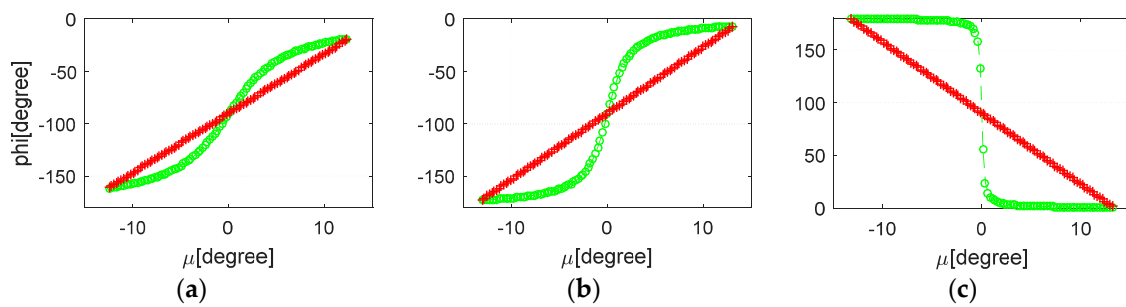


**Figure 4.** The yaw angle of G06 (IIF) during shadow crossing for different sun angles: (**a**) beta = $4.19°$; (**b**) beta = $1.58°$; and (**c**) beta = $-0.17°$. The nominal yaw angle is shown in green, while the modeled one is in red.

### 3.2.2. GLONASS-M Satellites

Different from the noon maneuver of GPS satellites, the GLONASS-M satellites do not start adjusting their attitude when the yaw rates exceed the maximum hardware yaw rates ($0.25°$/s), but start at a certain time before the noon maneuver, rotating with the maximum hardware yaw rates. The attitude is symmetrical distribution centered around the noon. The orbital angle of the start time ($\mu_s$) and the end time ($\mu_e$) of maneuver satisfy $\mu_s + \mu_e = 2\pi$. To calculate the start time and the end time, an iterative algorithm is needed [9]. As shown in Figure 5, the maximum yaw angle differences of the noon maneuver are smaller than that of the GPS satellites for the same beta angle. When the sun angle is approximately $0.05°$ in Figure 5c, the difference can be up to around $71.38°$ and the duration can be up to around 12 min.
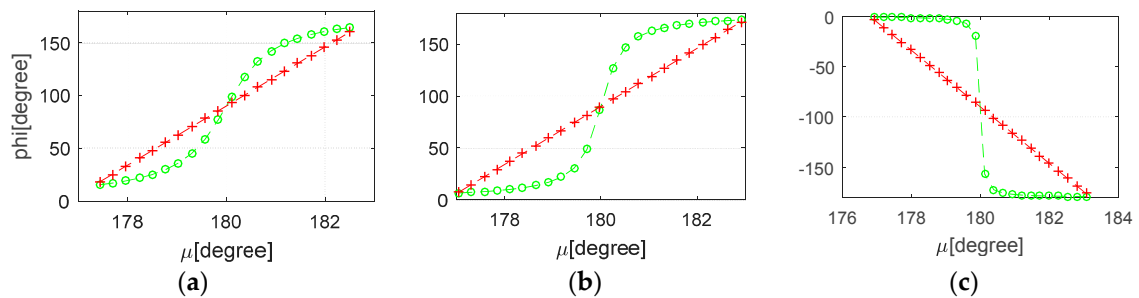


**Figure 5.** The yaw angle of R10 (M) during noon maneuver for different sun angles: (**a**) beta = $-0.70°$; (**b**) beta = $-0.33°$; and (**c**) beta = $0.05°$. The nominal yaw angle is shown in green, while the modeled one is in red.

As soon as the GLONASS-M satellites enter into the shadow crossing regime, they will rotate with the maximum hardware yaw rates so that the nominal attitude can be reached before the exit of the shadow crossing. The length of this period also depends on the value of the sun angle. Then, the attitude remains unchanged until out of the shadow crossing. As shown in Figure 6, the maximum yaw angle differences of the shadow crossing are significant bigger than those of the GPS IIF satellites for the same beta angle. Even the GLONASS-M satellite is at the shadow entry, as shown in Figure 6c, the maximum difference can be up to more than 20°. When the sun angle is small (0.24°), as shown in Figure 6a, the maximum difference can be up to about 180° and the duration can be up to about 53 min. Therefore, the influence of the shadow crossing for GLONASS-M satellites is apparently greater than that of the GPS satellites (including both the IIR and IIF satellites).
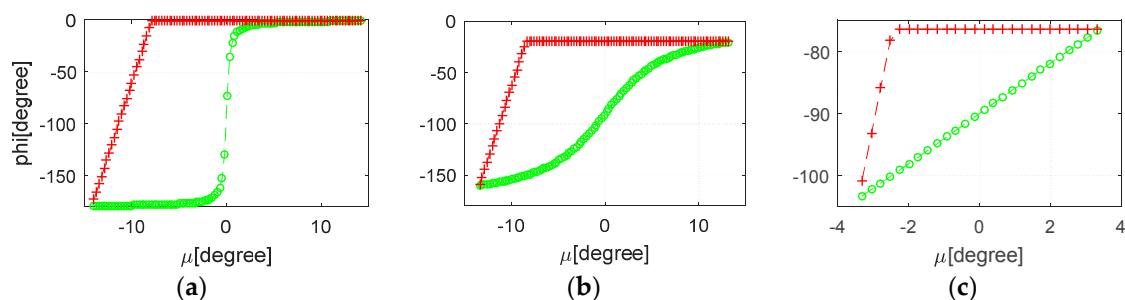


**Figure 6.** The yaw angle of R10 (M) during shadow crossing for different sun angles: (**a**) beta = 0.24°; (**b**) beta = 4.77°; and (**c**) beta = 13.79°. The nominal yaw angle is shown in green, while the modeled one is in red.

### 3.2.3. GALILEO-FOC Satellites

During the period of July 2017, no GALILEO IOV satellites are in eclipse. Therefore, only the yaw angle differences of GALILEO FOC satellites are analyzed. According to the official description, when the GALILEO-FOC satellites approach the orbit noon or the midnight, the modified yaw steering law is adopted to keep the yaw change rate low. Different from other satellite systems, the sign of the yaw angle rather than the sun angle, at the time of the switch, must be stored. As shown in Figure 7, the noon maneuver of GALILEO FOC satellites looks like that of the GLONASS-M satellites, whose attitudes are symmetrical distribution centered around the noon. The maximum duration of noon maneuver for GALILEO FOC satellites is about 47 min. During the first 7 min and the last 7 min of the noon maneuver, the nominal and the modeled yaw angles agree within a few degrees, even for a very small sun angle (0.02°). As shown in Figure 8, when the absolute sun angle is larger than 2.0°, the maximum differences will be within 20°.
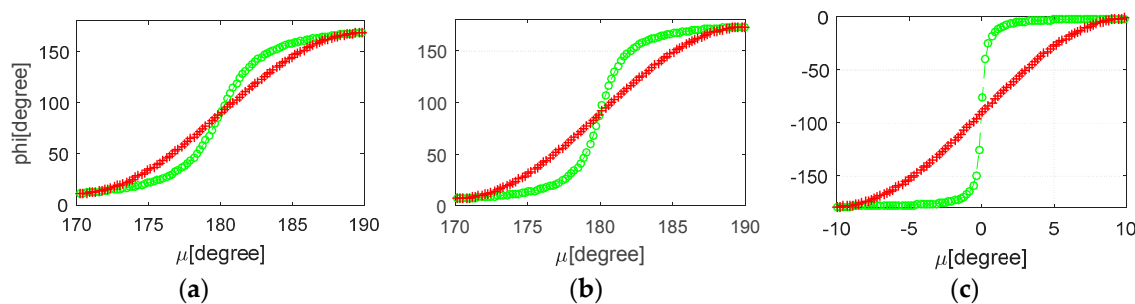


**Figure 7.** The yaw angle of E01 (FOC) during noon maneuver for different sun angles: (**a**) beta = −1.99°; (**b**) beta = −1.19°; and (**c**) beta = 0.02°. The nominal yaw angle is shown in green, while the modeled one is in red.
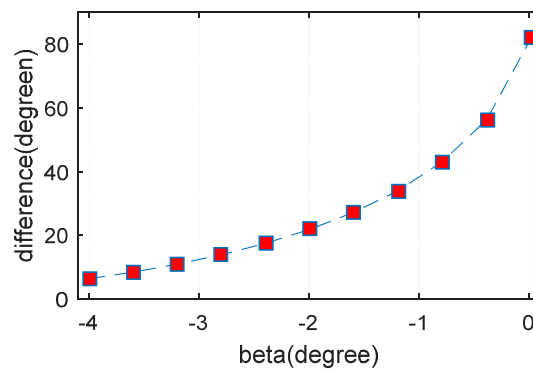
**Figure 8.** The yaw angle differences of E01 (FOC) during noon maneuver for different sun angles (−4.00° to 0.02°).

### 3.2.4. BDS Satellites

According to the empirical threshold for the attitude switch, as shown in Figure 9, C10 starts switching from yaw steering mode to the orbit normal mode at about 20:18:30 (7 July 2017). When the sun angle is very close to 4°, C10 does not switch its attitude mode immediately until its yaw angle approaches to 5°. At this time, the sun angle is about −3.6°. It is obvious that the yaw angle differences between these two attitude modes can be up to 180°. Due to the slow variation of the sun angle, the duration of the orbit normal mode can last for several days. Because of the few BDS MEO satellites and the large satellite PCO values, the non-nominal yaw attitude will have a great impact on the positioning of the BDS-only PPP.
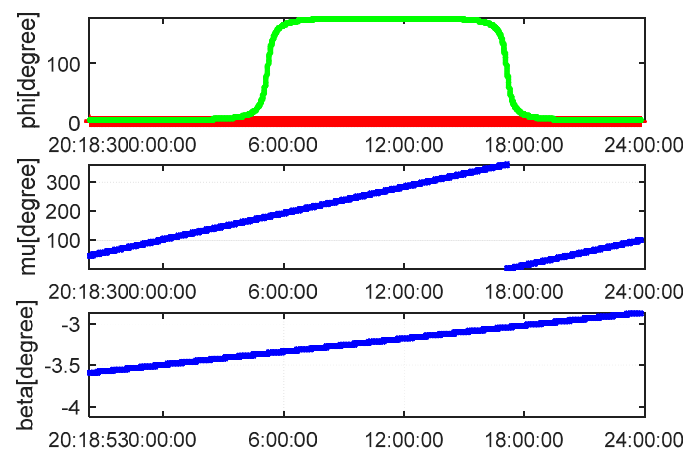


**Figure 9.** The attitude switch of BDS C10.

### 3.3. The Impact of Eclipsing Satellites on the GNSS PPP

To analyze the impact of the eclipsing satellites on GNSS PPP, as shown in Figure 10, the observation data of 65 MGEX stations for 31-day period in July 2017 are selected. All these stations can track GPS/GLONASS/GALILEO/BDS signals. Then, three eclipsing strategies are designed:

1. Strategy 1 (S1): delete all the eclipsing satellites;
2. Strategy 2 (S2): always use nominal attitude, even when this satellite is in eclipsing season; and
3. Strategy 3 (S3): use the modeled attitude when this satellite is in eclipsing season; otherwise, the nominal attitude is used.

In the subsequent subsection, the positioning accuracy, the observation residuals and the convergence time of these three eclipsing strategies are compared for the single-system PPP and GNSS PPP. All stations are used to conduct GPS-only PPP, GLONASS-only PPP and GNSS PPP in both static and kinematic mode. Because the number of GALILEO satellites is still small, only the static mode is performed for GALILEO-only PPP. Considered that the BDS satellites are mainly concentrated in the Asia Pacific Region, 10 stations marked as triangles are used to perform BDS-only PPP in both static and kinematic mode. The reference coordinates of these stations were given by IGS SINEX weekly solutions with an accuracy of a few millimeters. To ensure the positioning reliability, the convergence time is defined as the time required to achieve the 3D positioning error less than 10 cm for consecutive 20 epochs.
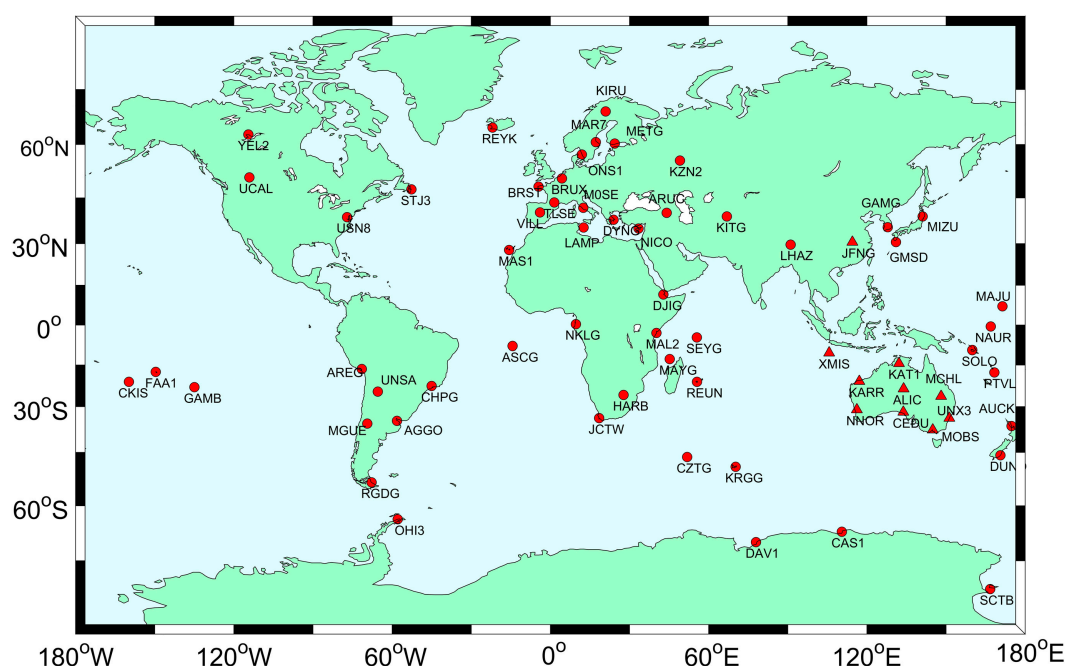


**Figure 10.** The distribution of the selected GNSS stations (as of July 2017).

### 3.3.1. The Impact on the Positioning Accuracy of the Single-System Static PPP

The filter solutions at current epoch are the weighted average values of the prediction values and the current measurements. When the filter is not converged, the contributions of current measurements to the filter solutions are relatively large. At this time, the effects of the eclipsing satellites will be highlighted, possibly resulting in a worse solution and a longer convergence time. Because the coordinate parameters in static PPP are set as constant models, when the filter is converged fully, the prediction values are relatively accurate and the effects of the eclipsing satellites are weakened.

The average RMS (Root Mean Square) values of the three eclipsing strategies for single-system PPP are shown in Table 6. The RMS computations for the north, east and up coordinate components are based on the positioning errors of all the converged epochs. For GPS-only static PPP, the positioning performances of three eclipsing strategies are almost the same. Compared to S2, the improvements of S1 and the S3 are trivial. Different from the GPS-only PPP, S1 and S3 of the GLONASS-only static PPP can achieve a better accuracy than that of S2. The improvements of S1 are 8.60%, 9.92% and 4.77% in the north, east and up direction, while the improvements of S3 are 11.20%, 12.3% and 6.43%, respectively. The main reasons for these improvements are the large PCO values and the long durations of the GLONASS satellites shadow crossing (54 min for GLONASS satellites). Due to the limited number of the visible satellites for the single-system PPP, deleting satellites may induce a poorer satellite

geometry structure. Therefore, the improvements of S3 are greater than S1. Because the released time of the official attitude control model for GALILEO FOC satellites is later than the experimental time in this contribution, the nominal attitude or the IOV satellites' attitude may be adopted for the FOC satellites in the estimation of the precise orbit and clock products used in PPP. Therefore, using official attitude will not result in a better solution than that of the nominal attitude. It is not hard to find that deleting GALILEO satellites may reduce the satellite geometric strength because, on average, only 4–6 GALILEO satellites can be tracked for one station. It is worth noting that the eclipsing satellites have the greatest impact on the BDS-only static PPP. Compared with S2, using the modeled attitude can improve the positioning accuracy by about 34.99%, 38.34% and 22.39% in the north, east and up direction, respectively. Furthermore, deleting BDS eclipsing satellites can also improve the accuracy by 19.20%, 22.56% and 12.16% in the north, east and up direction, respectively.

**Table 6.** The average RMS values (mm) under different scenarios.

| Constellation | Average Percentage | Direction | Static | | | Kinematic | | |
|---|---|---|---|---|---|---|---|---|
| | | | S1 | S2 | S3 | S1 | S2 | S3 |
| G | 9.2% (31) [1] | N | 4.25 | 4.24 | 4.20 | 16.80 | 16.89 | 16.76 |
| | | E | 8.49 | 8.56 | 8.49 | 24.13 | 24.15 | 24.01 |
| | | U | 10.35 | 10.42 | 10.32 | 41.56 | 41.68 | 41.40 |
| R | 27.3% (22) | N | 5.63 | 6.16 | 5.47 | 43.38 | 43.33 | 38.33 |
| | | E | 11.26 | 12.50 | 10.96 | 71.72 | 73.49 | 65.97 |
| | | U | 12.57 | 13.20 | 12.35 | 106.40 | 112.07 | 99.12 |
| E [2] | 22.2% (18) | N | 7.63 | 7.56 | 7.58 | - | - | - |
| | | E | 15.78 | 15.50 | 15.56 | - | - | - |
| | | U | 26.33 | 25.76 | 25.86 | - | - | - |
| C [3] | 14.3% (14) | N | 8.96 | 11.09 | 7.21 | 34.71 | 49.20 | 22.83 |
| | | E | 15.41 | 19.90 | 12.27 | 40.73 | 64.52 | 30.84 |
| | | U | 24.56 | 27.96 | 21.70 | 95.09 | 165.78 | 68.02 |
| GR | 16.6% (53) | N | 3.77 | 3.77 | 3.75 | 11.44 | 11.64 | 11.27 |
| | | E | 6.57 | 6.56 | 6.57 | 15.63 | 15.79 | 15.53 |
| | | U | 8.58 | 8.61 | 8.56 | 29.47 | 30.21 | 29.33 |
| GREC | 13.0% (85) | N | 3.62 | 3.61 | 3.61 | 10.18 | 10.23 | 10.11 |
| | | E | 5.94 | 5.96 | 5.95 | 13.41 | 13.46 | 13.23 |
| | | U | 8.53 | 8.55 | 8.53 | 26.28 | 26.40 | 26.08 |

[1] The data in the parentheses represent the number of operational satellites of this constellation. [2] Because the period when GALILEO satellites enter into the eclipsing regimes are mainly from 12 to 23 July, the results of GALILEO-only PPP are referred to these periods. [3] Because the period when BDS satellites enter into the eclipsing regimes are mainly from 8 to 20 July, the results of BDS-only PPP are referred to these periods.

To further analyze the reason of the significant improvement for the BDS-only static PPP, the positioning performance of three eclipsing strategies and the phase residuals of S2 are shown in Figures 11 and 12. At the observation time, two BDS IGSO satellites are in eclipse. Their actual yaw angles are zero and the maximum yaw angle differences are 180°. Due to the smaller average orbital angular velocity (0.00418°/s) of BDS IGSO satellites, the duration for maximum yaw angle differences is rather long, usually lasting for about several hours. At this time, large systematic errors caused by the non-nominal attitude will be brought into the phase residuals. The maximum residuals will reach up to 13 cm during the process of the filter convergence, which result in big deviations in the positioning solutions. This will also influence the positioning accuracy of the subsequent epochs for a long time, even after the convergence. It is also obvious to find that deleting these eclipsing satellites will induce a longer convergence time. Due to the smaller variation of the BDS satellites geometry structure, this phenomenon will be more obvious than other satellite systems.
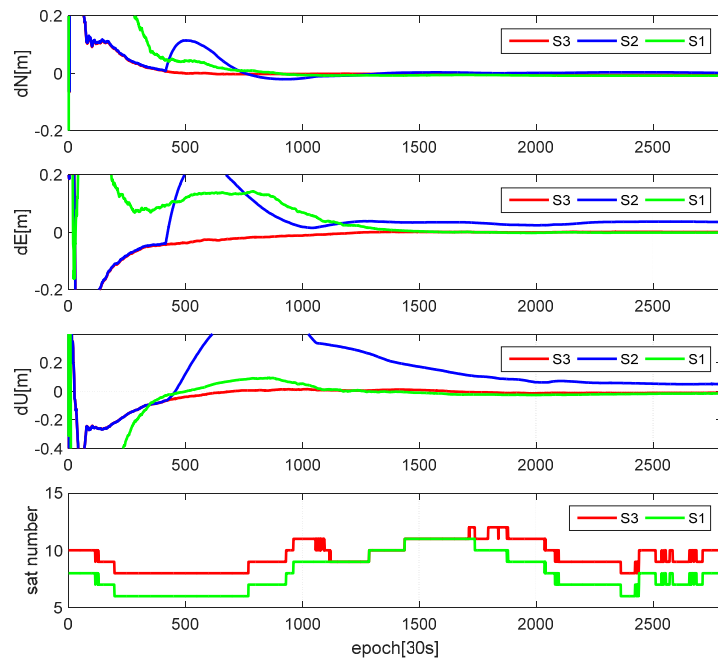
**Figure 11.** The positioning performance of BDS-only static PPP for three eclipsing strategies (JFNG station, DOY 195 of 2017, the sampling rate is 30 s).



(a)
(b)
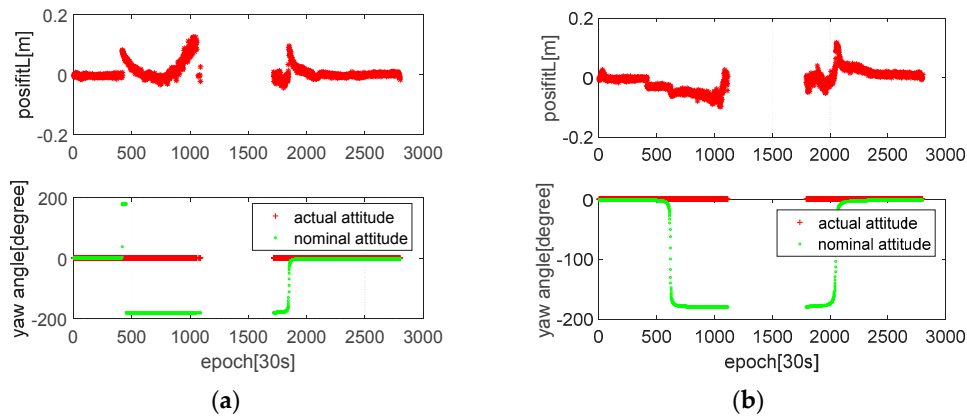
**Figure 12.** The phase residuals of: BDS C07 (**a**); and C10 (**b**) with strategy 2 (JFNG station, DOY 195 of 2017, the sampling rate is 30 s).

3.3.2. The Impact on the Positioning Accuracy of the Single-System Kinematic PPP

Different from the static PPP, the coordinate parameters will be set as the white noise model (or random-walk model in low dynamic environment). The strength of the mathematic model is reduced and more number of visible satellites is required. As shown in Table 6, because the tracked GPS satellites are usually enough, S2 can achieve nearly the same positioning performance as that of S3. Compared with S2, the improvements of S1 and S3 are also trivial. This is mainly because of the decommission of II/IIA satellites and the limited number of the IIF satellites (12 IIF satellites among all 32 GPS satellites). Therefore, the impact of the tracked eclipsing IIF satellites will be weakened. S1 and S3 of the GLONASS-only kinematic PPP can achieve a better accuracy than that of S2. The improvements of S1 are 0.12%, 2.41% and 5.06% in the north, east and up direction, while the improvements of S3 are 11.54%, 10.23% and 11.56%, respectively. Unlike GPS, the GLONASS GDOP is usually smaller in the high latitude regions (larger than $45°$) than the other regions [40]. Therefore,

deleting the GLONASS eclipsing satellites for the station located in the middle or low latitude may greatly reduce its geometric strength. Three stations, namely RGDG (South 53.79°), MGUE (South 35.78°) and AREG (South 16.47°), with nearly the same longitude are selected. As shown in Figure 13, the positioning performance of GLONASS kinematic PPP is clearly related to the latitude of the station. The positioning performance of S1 and S2 of the station RGDG are nearly the same, however, this is not the case for the station MGUE and AREG. It is apparent to find that deleting eclipsing satellites will not always ensure a better solution, even resulting a worse solution than that of S2. Therefore, the mean improvement for all the stations of S2 is obviously smaller than that of S3. Similar to the BDS static PPP, the eclipsing satellites have the greatest impact on the BDS-only kinematic PPP. Compared with S2, using the modeled attitude can improve the positioning accuracy by about 53.59%, 52.20% and 58.96% in the north, east and up direction, respectively, while deleting BDS eclipsing satellites can improve the accuracy by 29.45%, 36.87% and 42.64% in the north, east and up direction, respectively. This is also because of the long duration of maximum yaw angle differences, large PCO values and the limited number of visible satellites.
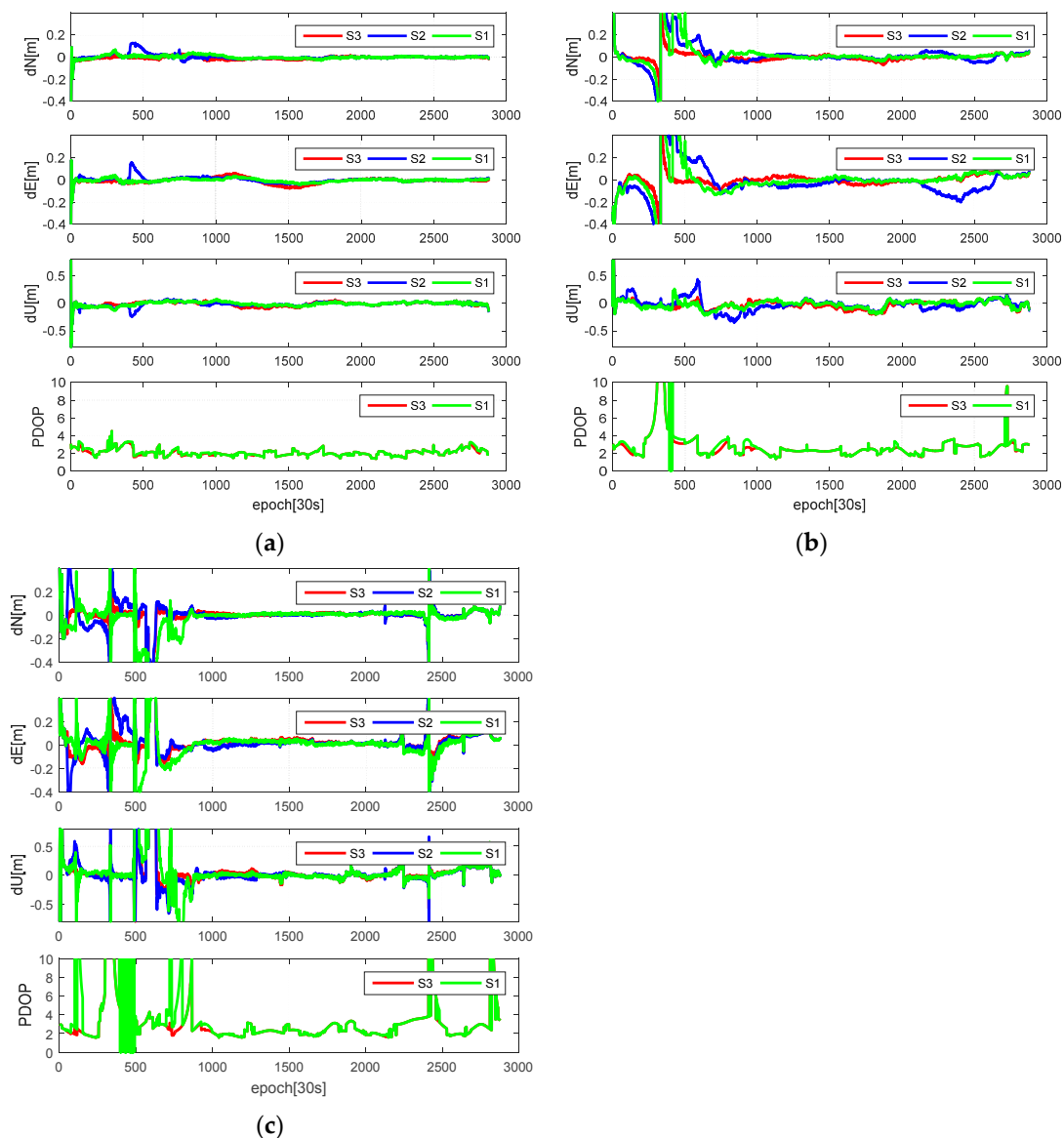


**Figure 13.** The positioning performance of GLONASS-only kinematic PPP for three eclipsing strategies: (**a**) station RGDG; (**b**) station MGUE; and (**c**) station AREG (DOY 194 of 2017, the sampling rate is 30 s).

### 3.3.3. The Relationship between the Sun Angle and the Accuracy Improvement

From the above analysis, the impact of the eclipsing satellites on the positioning accuracy is related to the magnitude of the PCO values, the maximum yaw angle differences, the duration of noon maneuver or the shadow crossing and satellite geometry structure. However, the maximum yaw angle differences and the duration of noon maneuver or the shadow crossing are related to the sun angles. Due to the large positioning accuracy improvement of S3 relative to S2 for the GLONASS-only and BDS-only PPP, the improvement of 3D positioning accuracy for every day in July 2017 are shown in Figure 14. For GLONASS, according to the results of the eclipsing monitor, the improvement becomes smaller as the sun angle becomes bigger. Because the tracked satellites of every day are different (the nominal orbital repeat period for GLONASS satellites is eight days) and the improvements of every station are also different, the mean improvements for all stations of every day do not necessarily conform to the above rules. When the sun angles of GLONASS satellites approach to the sun angle limit of the earth shadow (14.2°), the accuracy improvement is vital. Because BDS adopts the normal orbit mode and yaw steering mode, as soon as the attitudes of BDS satellites are switching to the normal orbit mode, the improvements become large, even when their sun angles are near 4°.
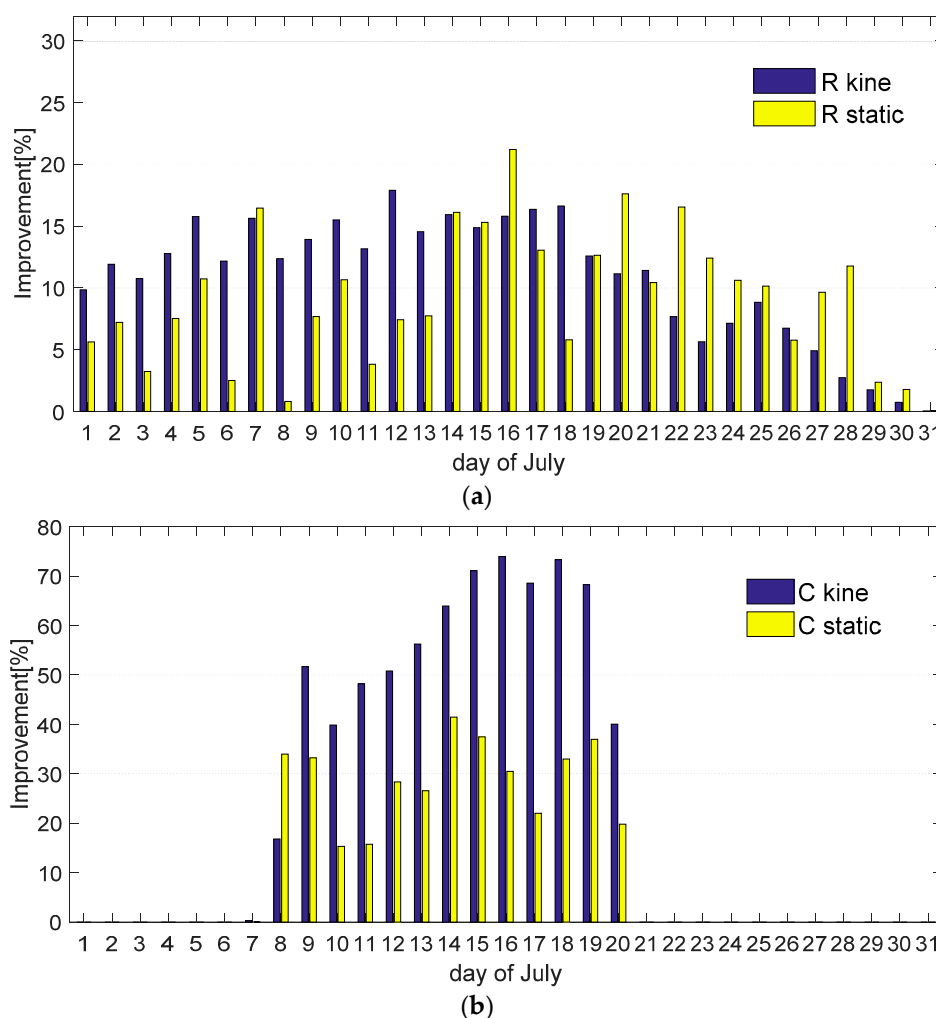


**Figure 14.** The 3D positioning accuracy improvements of S3 relative to S2 for every day in July 2017: (**a**) GLONASS-only PPP; and (**b**) BDS-only PPP. The dark blue represents the PPP dynamic mode while the yellow represents the PPP static mode.

### 3.3.4. The Effect of the Satellite Geometry Structure

From the above analysis, the number of the visible satellites will significant influence the positioning accuracy and the convergence time for the single-system PPP, especially for the GLONASS-only (except stations in the high latitude regions) or BDS-only kinematic PPP mode.

First, the number of eclipsing satellites for each system are investigated. In general, the satellites on the same orbital plane will successively enter into the eclipsing regimes, and the eclipsing period for more than one orbital plane happens very rarely. There are about 4–6 satellites distributed in one orbital plane for GPS. Due to the different sun angle limits of GPS IIR and IIF satellites, all GPS satellites on the same orbital plane will not be in the eclipsing period at the same time. The average percentage of eclipsing satellites for every day in July (the ration of the number of eclipsing satellites to that of all the constellation) can be computed according to the eclipsing monitoring results. As shown in the second column of Table 6, the average percentage of GPS among all the July is about 9.2% (approximately three GPS satellites). In the case of GLONASS, there are only three orbital planes, which means that the whole orbital plane (generally, in total eight satellites) are in the eclipsing period at the same time. During the experimental time, the average percentage of GLONASS among all the July is about 27.3%. This large proportion can also be accounted for the great influences of eclipsing satellites on the GLONASS-only PPP. Since the GALILEO and BDS are still at the stage of development, the number of satellites of each orbital plane are usually smaller than that of GPS/GLONASS.

With the increasing number of the satellites, the geometric strength of the mathematical model is enhanced. At this time, the influence of the small amount of the eclipsing satellites will be weakened, especially for static PPP mode. As shown in the last six rows of Table 6, when multi-GNSS data are introduced into the PPP model, the positioning results of these three strategies are consistent in the static PPP mode. Different from the single-system kinematic PPP, deleting eclipsing satellites or using the modeled attitudes will slightly improve the multi-GNSS PPP positioning results. Compared with Figure 13c, the PDOP of GR in station AREG, shown in Figure 15, is so small that deleting eclipsing satellites will not result in a worse solution. The improvements of S3 in GR kinematic PPP mode are 3.18%, 1.64% and 2.91% in the north, east and up direction while the improvements of S3 in GREC kinematic PPP mode are 1.17%, 1.71% and 1.21%, respectively. As shown in the second column of Table 6, the percentage of the GPS/GLONASS eclipsing satellites is smaller than that of GLONASS. When data of four satellite system are available, the percentage of the eclipsing satellites is further decreased to 13%. The enough non-eclipsing satellites are benefit for decreasing the influences of the non-nominal attitudes. Therefore, the improvements of S1 and S2 are decreased with the satellite geometric strength. When observations of four systems are available, the improvements are non-significant.

To further analyze the effect of the satellite geometry structure, the average convergence time and the percentage of convergence under different sessions (30 min and 60 min) are also shown in Table 7. For GPS-only PPP, deleting eclipsing satellites is helpful to improve the positioning accuracy, however, the mean convergence time is also affected and becomes slightly longer than that of S2. When it comes to multi-GNSS PPP mode, the mean convergence time of PPP is greatly reduced and the percentage of convergence within 30 min is also significantly increased. Compared with S2, both S1 and S3 of GR PPP can slightly reduce the mean convergence time. When data of the GALILEO and BDS are also introduced into PPP model, the reduction of the convergence time becomes further smaller. One of the reason for this slight reduction is that only when eclipsing satellites appear in the stage of the convergence may influence the convergence time.
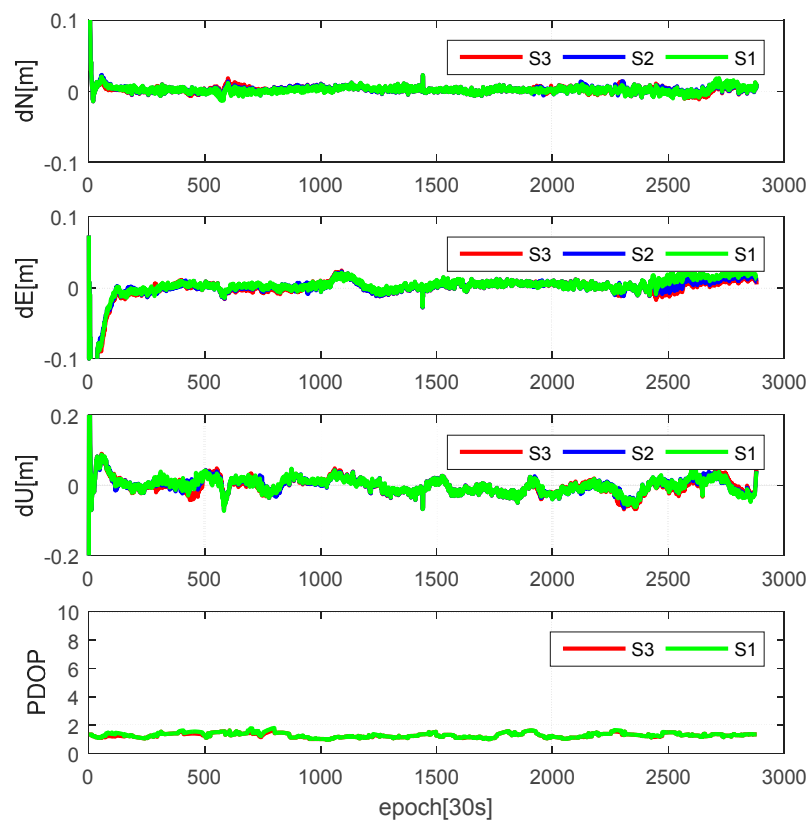
**Figure 15.** The positioning performance of GR kinematic PPP for three eclipsing strategies. (Station AREG, DOY 194 of 2017, the sampling rate is 30 s).

**Table 7.** The average convergence time (minute) and the percentage of convergence under different session length (30 min and 60 min).

| Constellation | Duration | Static | | | Kinematic | | |
|---|---|---|---|---|---|---|---|
| | | S1 | S2 | S3 | S1 | S2 | S3 |
| G | 30 | 72.48% | 73.06% | 73.65% | 35.69% | 36.69% | 37.47% |
| | 60 | 95.37% | 95.88% | 96.34% | 74.82% | 75.83% | 77.14% |
| | mean | 33.02 | 32.63 | 32.35 | 55.54 | 54.97 | 53.71 |
| GR | 30 | 94.21% | 94.26% | 94.36% | 84.65% | 83.91% | 84.65% |
| | 60 | 99.75% | 99.75% | 99.80% | 98.68% | 98.73% | 98.78% |
| | mean | 23.82 | 23.89 | 23.68 | 28.21 | 28.47 | 28.15 |
| GREC | 30 | 96.40% | 96.80% | 96.70% | 92.56% | 92.25% | 92.98% |
| | 60 | 99.85% | 99.99% | 99.99% | 99.85% | 99.80% | 99.85% |
| | mean | 22.11 | 21.76 | 21.95 | 24.94 | 24.97 | 24.81 |

## 4. Conclusions

The attitudes of GNSS satellites are the critical information for GNSS precise point positioning, especially when the orbit products are referred to the center of mass. After monitoring the sun angles and the orbital angles for all GNSS satellites, it has been found that 18 satellites are in eclipse in July 2017. The maximum yaw angle differences and the duration of maneuver for these satellites are analyzed. Datasets collected from 65 globally distributed MGEX stations in July 2017 are selected to analyze the influences of the eclipsing satellites on the single-system and multi-system PPP. The positioning results of three eclipsing strategies, including deleting eclipsing satellites (S1), always using nominal attitudes (S2) and using modeled attitudes (S3), are compared. The results show that the influences of

non-nominal attitudes are related to the magnitude of the PCO values, maximum yaw angle differences, the duration of maneuver, the value of the sun angle and the satellite geometric strength.

For GPS-only static or kinematic PPP, the accuracy improvement of S1 and S3 is non-vital. This is because: (1) the GPS IIA satellites are decommissioned from current GPS constellation; (2) the PCO values of IIR satellites are nearly zero; and (3) the number of visible IIF satellites for one station is limited. Due to the large PCO values and the long durations of the GLONASS satellites shadow crossing (54 min for GLONASS satellites), S1 and S3 of the GLONASS-only PPP can achieve a better accuracy than that of S2. For GLONASS-only static PPP model, the improvements of S1 are 8.60%, 9.92% and 4.77% in the north, east and up direction, while the improvements of S3 are 11.20%, 12.3% and 6.43%, respectively. For GLONASS-only kinematic PPP model, the improvements of S1 are 0.12%, 2.41% and 5.06% in the north, east and up direction, while the improvements of S3 are 11.54%, 10.23% and 11.56%, respectively. Because the inconsistency of the modeled attitudes of GALILEO FOC satellites and the underlying attitudes in the precise clock products, using official attitude will result in a slightly worse solution than that of the nominal attitude. Because of the long duration of maximum yaw angle differences, large PCO values and the limited number of visible satellites, both the BDS-only static and kinematic PPP using the modeled attitudes can greatly improve the positioning accuracy. The improvements of S3 for BDS-only static PPP are about 34.99%, 38.34% and 22.39% in the north, east and up direction, while for BDS-only kinematic PPP are about 53.59%, 52.20% and 58.96%, respectively.

Due to the poor satellite geometry of GLONASS-only kinematic (especially when stations are located in the low or the middle latitude) and BDS-only kinematic PPP, deleting eclipsing satellites will not always ensure a better solution, even resulting a worse solution than that of S2. This situation can be solved when multi-GNSS data are available. With the increase of the satellite geometric strength, the accuracy improvement is gradually reduced. When data of four systems are introduced into PPP model, the slight improvements of S1 and S3 are nearly the same. In the future, when the modeled attitudes are more consistent with the actual attitude control model, especially for GALILEO FOC satellites, the positioning accuracy of single-system PPP will be further improved, which also benefits the multi-GNSS PPP.

**Author Contributions:** Xinyun Cao and Shoujian Zhang conceived and designed the experiments; Xinyun Cao performed the experiments; Xinyun Cao and Tianjun Liu analyzed the data; Kaifa Kuang and Kang Gao contributed analysis tools; and Xinyun Cao wrote the paper.

**Conflicts of Interest:** The authors declare no conflict of interest.

## References

1. Bar-Sever, Y.E. A new model for GPS yaw attitude. *J. Geod.* **1996**, *70*, 714–723. [CrossRef]
2. Montenbruck, O.; Peter, S.; André, H. Broadcast versus precise ephemerides: A multi-GNSS perspective. *GPS Solut.* **2015**, *19*, 321–333. [CrossRef]
3. Montenbruck, O.; Schmid, R.; Mercier, F.; Steigenberger, P.; Noll, C.; Fatkulin, R.; Kogure, S.; Ganeshan, A.S. GNSS satellite geometry and attitude models. *Adv. Space Res.* **2015**, *56*, 1015–1029. [CrossRef]
4. Dow, J.M.; Neilan, R.E.; Rizos, C. The international GNSS service in a changing landscape of global navigation satellite systems. *J. Geod.* **2009**, *83*, 191–198. [CrossRef]
5. Kouba, J. A simplified yaw-attitude model for eclipsing GPS satellites. *GPS Solut.* **2009**, *13*, 1–12. [CrossRef]
6. Dilssner, F. GPS IIF-1 satellite antenna phase center and attitude modeling. *Inside GNSS* **2010**, *5*, 59–64.
7. Dilssner, F.; Springer, T.; Enderle, W. GPS IIF yaw attitude control during eclipse season. In Proceedings of the AGU Fall Meeting, San Francisco, CA, USA, 5–9 December 2011.
8. Kuang, D.; Desai, S.; Sibois, A. Observed features of GPS Block IIF satellite yaw maneuvers and corresponding modeling. *GPS Solut.* **2017**, *21*, 739–745. [CrossRef]

9.　Dilssner, F.; Springer, T.; Gienger, G.; Dow, J. The GLONASS-M satellite yaw-attitude model. *Adv. Space Res.* **2011**, *47*, 160–171. [CrossRef]

10.　Galileo Satellite Metadata. Available online: https://www.gsc-europa.eu/support-to-developers/galileo-satellite-metadata#9 (accessed on 6 October 2017).

11.　Guo, J.; Zhao, Q.; Geng, T.; Xu, S.; Liu, J. Precise orbit determination for COMPASS IGSO satellites during yaw maneuvers. In Proceedings of the China Satellite Navigation Conference (CSNC), Wuhan, China, 15–17 May 2013; pp. 41–53.

12.　Dai, X.; Ge, M.; Lou, Y.; Shi, C.; Wickert, J.; Schuh, H. Estimating the yaw-attitude of BDS IGSO and MEO satellites. *J. Geod.* **2015**, *89*, 1005–1018. [CrossRef]

13.　Zhao, Q.; Wang, C.; Guo, J.; Wang, B.; Liu, J. Precise orbit and clock determination for BeiDou-3 experimental satellites with yaw attitude analysis. *GPS Solut.* **2018**, *22*, 4. [CrossRef]

14.　Ge, M.; Gendt, G.; Rothacher, M.; Shi, C.; Liu, J. Resolution of GPS carrier-phase ambiguities in precise point positioning (PPP) with daily observations. *J. Geod.* **2008**, *82*, 389–399. [CrossRef]

15.　Zumberge, J.F.; Heflin, M.B.; Jefferson, D.C.; Watkins, M.M.; Webb, F.H. Precise point positioning for the efficient and robust analysis of GPS data from large networks. *J. Geophys. Res.* **1997**, *102*, 5005–5017. [CrossRef]

16.　Li, X.; Ge, M.; Zhang, X.; Zhang, Y.; Guo, B.; Wang, R.; Wickert, J. Real-time high-rate co-seismic displacement from ambiguity-fixed precise point positioning: Application to earthquake early warning. *Geophys. Res. Lett.* **2013**, *40*, 295–300. [CrossRef]

17.　Geng, J.; Teferle, F.N.; Meng, X.; Dodson, A. Kinematic precise point positioning at remote marine platforms. *GPS Solut.* **2010**, *14*, 343–350. [CrossRef]

18.　Lou, Y.; Zheng, F.; Gu, S.; Liu, J. The Impact of Non-nominal Yaw Attitudes of GPS Satellites on Kinematic PPP Solutions and their Mitigation Strategies. *J. Navig.* **2015**, *68*, 718–734. [CrossRef]

19.　Montenbruck, O.; Steigenberger, P.; Prange, L.; Deng, Z.; Zhao, Q.; Perosanz, F.; Romero, I.; Noll, C.; Stürze, A.; Weber, G.; et al. The multi-GNSS experiment (MGEX) of the international GNSS service (IGS)—Achievements, prospects and challenges. *Adv. Space Res.* **2017**, *59*, 1671–1697. [CrossRef]

20.　Lou, Y.; Zheng, F.; Gu, S.; Wang, C.; Guo, H.; Feng, Y. Multi-GNSS precise point positioning with raw single-frequency and dual-frequency measurement models. *GPS Solut.* **2016**, *20*, 849–862. [CrossRef]

21.　Li, X.; Ge, M.; Dai, X.; Ren, X.; Fritsche, M.; Wickert, J.; Schuh, H. Accuracy and reliability of multi-GNSS real-time precise positioning: GPS, GLONASS, BeiDou, and Galileo. *J. Geod.* **2015**, *89*, 607–635. [CrossRef]

22.　Liu, T.; Yuan, Y.; Zhang, B.; Wang, N.; Tan, B.; Chen, Y. Multi-GNSS precise point positioning (MGPPP) using raw observations. *J. Geod.* **2017**, *91*, 253–268. [CrossRef]

23.　Arnold, D.; Meindl, M.; Beutler, G.; Dach, R.; Schaer, S.; Lutz, S.; Prange, L.; Sośnica, K.; Mervart, L.; Jäggi, A. CODE's new solar radiation pressure model for GNSS orbit determination. *J. Geod.* **2015**, *89*, 775–791. [CrossRef]

24.　The Average JPL Reporcessing Yaw-Rate Solutions. Available online: http://acc.igs.org/orbits/yrates.pdf (accessed on 1 July 2017).

25.　IGS and RTCM-SC104 (2015) RINEX—The Receiver Independent Exchange Format, Version 3.03, 14 July. International GNSS Service (IGS), RINEX Working Group and Radio Technical Commission for Maritime Service Special Committee. Available online: ftp://igs.org/pub/data/format/rinex303.pdf (accessed on 14 July 2015).

26.　Cai, C.; Gao, Y. Modeling and assessment of combined GPS/GLONASS precise point positioning. *GPS Solut.* **2013**, *17*, 223–236. [CrossRef]

27.　Li, P.; Zhang, X.; Guo, F. Ambiguity resolved precise point positioning with GPS and BeiDou. *J. Geod.* **2017**, *91*, 25–40.

28.　Guo, F.; Li, X.; Zhang, X.; Wang, J. Assessment of precise orbit and clock products for Galileo, BeiDou, and QZSS from IGS Multi-GNSS Experiment (MGEX). *GPS Solut.* **2017**, *21*, 279–290. [CrossRef]

29.　Wanninger, L.; Beer, S. BeiDou satellite-induced code pseudorange variations: Diagnosis and therapy. *GPS Solut.* **2015**, *19*, 639–648.

30.　Gao, Y.; Lahaye, F.; Heroux, P.; Liao, X.; Beck, N.; Olynik, M. Modeling and estimation of C1–P1 bias in GPS receivers. *J. Geod.* **2001**, *74*, 621–626. [CrossRef]

31.　Blewitt, G. An automatic editing algorithm for GPS data. *Geophys. Res. Lett.* **1990**, *17*, 199–202. [CrossRef]

32.　Yang, Y.; Song, L.; Xu, T. Robust estimator for correlated observations based on bifactor equivalent weights. *J. Geod.* **2002**, *76*, 353–358. [CrossRef]

33. Lagler, K.; Schindelegger, M.; Böhm, J.; Krásná, H.; Nilsson, T. GPT2: Empirical slant delay model for radio space geodetic techniques. *Geophys. Res. Lett.* **2013**, *40*, 1069–1073. [CrossRef] [PubMed]

34. Hadas, T.; Krypiak Gregorczyk, A.; Hernández Pajares, M.; Kaplon, J.; Paziewski, J.; Wielgosz, P.; Garcia Rigo, A.; Kazmierski, K.; Sosnica, K.; Kwasniak, D.; et al. Impact and Implementation of Higher-Order Ionospheric Effects on Precise GNSS Applications. *J. Geophys. Res.-Solid Earth* **2017**, *122*, 9420–9436. [CrossRef]

35. Guo, J.; Xu, X.; Zhao, Q.; Liu, J. Precise orbit determination for quad-constellation satellites at Wuhan University: Strategy, result validation, and comparison. *J. Geod.* **2016**, *90*, 143–159. [CrossRef]

36. Petit, G.; Luzum, B. IERS Conventions (2010). Bureau International des Poids et Mesures Sevres (France). 2010. Available online: https://www.iers.org/IERS/EN/Publications/TechnicalNotes/tn36.html (accessed on 1 July 2017).

37. Wu, J.T.; Wu, S.C.; Hajj, G.A.; Bertiger, W.I.; Lichten, S.M. Effects of antenna orientation on GPS carrier phase. In Proceedings of the AAS/AIAA Astrodynamics Conference, San Diego, CA, USA, 19–22 August 1992; pp. 1647–1660.

38. Montenbruck, O.; Hauschild, A.; Steigenberger, P. Differential Code Bias Estimation using Multi-GNSS Observations and Global Ionosphere Maps. *Navigation* **2014**, *61*, 191–201. [CrossRef]

39. The GLONASS Constellation Status. Available online: https://www.glonass-iac.ru/en/GLONASS/ (accessed on 1 July 2017).

40. Zhou, F.; Dong, D.; Ge, M.; Li, P.; Wickert, J.; Schuh, H. Simultaneous estimation of GLONASS pseudorange inter-frequency biases in precise point positioning using undifferenced and uncombined observations. *GPS Solut.* **2018**, *22*, 19. [CrossRef]